

A Double-Threshold Technique for Fast Time-Correspondence Imaging

Ming-Fei Li, Yu-Ran Zhang, Heng Fan, and Ling-An Wu*

Institute of Physics, Chinese Academy of Sciences, Beijing 100190, China

Xue-Feng Liu and Xu-Ri Yao

Center for Space Science and Applied Research, Chinese Academy of Sciences, Beijing 100190, China

Kai-Hong Luo

Institute of Physics, Chinese Academy of Sciences, Beijing 100190, China and

*Integrated Quantum Optics, Applied Physics, University of Paderborn,
Warburger Str. 100, D-33098, Paderborn, Germany*

(Dated: July 11, 2018)

We present a robust imaging method based on time-correspondence imaging and normalized ghost imaging (GI) that sets two thresholds to select the reference frame exposures for image reconstruction. This double-threshold time-correspondence imaging protocol always gives better quality and signal-to-noise ratio than previous GI schemes, and is insensitive to surrounding noise. Moreover, only simple add and minus operations are required while less data storage space and computing time are consumed, thus faster imaging speeds are attainable. The protocol offers a general approach applicable to all GI techniques, and marks a further step forward towards real-time practical applications of correlation imaging.

[DOI : 10.1063/1.4832328]

PACS numbers: 42.30.Va, 42.0.Ar, 42.50.St

“Ghost” imaging (GI) was so named due to its surprising “nonlocal” feature, in which the image of an object was retrieved through the second-order quantum correlation between pairs of photons produced by spontaneous parametric down-conversion [1, 2]. However, GI with thermal light has also been demonstrated theoretically and experimentally [3–7] and has been interpreted successfully in terms of classical statistical optics [8, 9]. The controversy about whether GI is a quantum or classical phenomenon aroused a hot debate [10–15], but all agree that it has several advantages for practical applications. (1) Images of an unknown object may be obtained in a “nonlocal” manner, which can be used in remote sensing [16]; (2) the spatial resolution in GI may exceed the diffraction limit [17]; (3) GI can be performed with a true thermal light source without using a lens [18], which is useful in x-ray imaging [19]; (4) imaging is possible even in a turbulent atmosphere [20–23] or scattering medium [24, 25] under certain conditions.

However, some limitations still exist; notably, the visibility and signal-to-noise ratio (SNR) of thermal light GI is low, especially for complex gray-scale objects. Also, the image cannot be retrieved instantaneously, since it is based on averaging of the second-order correlation of two measurements, so a huge amount of data is involved. Happily, these shortcomings are not unsolvable. The quality can be improved using the techniques of differential ghost imaging (DGI) [26] and normalized ghost imaging (NGI) [27], by means of which the SNR of conventional GI can be enhanced enormously, although huge amounts of data and more complex computation are required. Ghost imaging via compressive sensing has been demonstrated which can give a high SNR with many fewer exposure frames [28, 29], but more computation time is necessary; sparsity constraints also limit its applications. Thus, less data acquisition, shorter computation times and high SNR are the ultimate goal of GI. Recently in our group, Luo *et al.* [30] reported a so-called correspondence imaging (CI) protocol which seemed to defy intuition in that no direct second-order correlation calculation is performed, while compared with conventional GI the number of exposures used to reconstruct the images and consequently the computation time are greatly reduced. This was then combined with DGI, i.e. time-correspondence differential GI, by which means high quality images were retrieved using only part of the reference detector data without computing the correlation function [31]. Although high efficiency and good quality images were obtained by setting two thresholds, it was not specified how the two thresholds should be set. In another work, high visibility ghost images were produced using a synthesized light source with exceptionally large

*Electronic address: wula@iphy.ac.cn

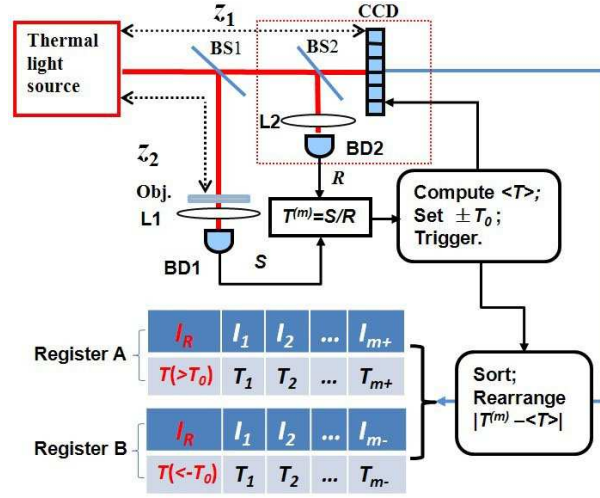


FIG. 1: (Color online). Schematic of experimental setup. BS1, BS2 beamsplitters, BD1, BD2 bucket detectors, Obj object, L1, L2 collection lenses, CCD spatially resolving reference camera, S bucket signal, R total reference intensity at BD2. A and B are computer registers.

intensity fluctuations, produced by means of a spatial light modulator [32]. Different from the above two methods, in this paper, instead of modifying the light source, we employ a special detection system which only picks out the large fluctuation signals and discards the small fluctuations, thus computational time and storage space can both be saved.

This approach, which we call double-threshold time-correspondence imaging (DTTCI), can be applied to all types of correlation imaging, while incorporating all their advantages. First, the image quality is better than that of traditional GI. Second, the method is insensitive to surrounding noise. Third, less exposure frames are needed to recover the image so imaging time and memory storage are reduced. Fourth, the computer algorithm is simple, so computation time is saved. With all these advantages, our method should be very useful in real practical applications.

The experimental setup, shown in Fig. 1, is a generic lensless GI system using thermal light, but with a second beamsplitter BS2 and bucket detector BD2 in the reference beam. The purpose of BD2 is to record the total intensity arriving at the reference detector CCD, and BS1 is assumed to be a 1:2 beamsplitter, while BS2 is a 50/50 one. The distances z_1 and z_2 from the light source to the CCD and object must be equal for lensless GI.

In conventional GI, the image is recovered from the second-order correlation function of the intensity fluctuations at two detectors, one of which only measures the total light transmitted through the object, while the other in an empty reference arm is capable of spatial resolution:

$$GI = \langle \delta S \delta I_R(\mathbf{x}_R) \rangle \simeq C_0 T(\mathbf{x}_R), \quad (1)$$

where S is the total intensity recorded by the object arm bucket detector, $I_R(\mathbf{x}_R)$ is the spatial distribution of the light intensity at the reference detector, \mathbf{x}_R denotes the spatial position, $C_0 = A_{coh} \langle I_R(\mathbf{x}_R) \rangle \langle I_B(\mathbf{x}_B) \rangle$ is a constant, A_{coh} is the average speckle size, and $T(\mathbf{x})$ the intensity transmission function of the object. The bucket signal S in the object beam is defined as [26, 27]

$$S = \int I_B(\mathbf{x}_B) T(\mathbf{x}_B) d^2 \mathbf{x}_B, \quad (2)$$

and $\delta S = S - \langle S \rangle$, $\delta I_R(\mathbf{x}_R) = I_R(\mathbf{x}_R) - \langle I_R(\mathbf{x}_R) \rangle$. The suffixes B and R denote bucket and reference arms, respectively. We also define the total reference signal in BD2 to be

$$R = \int I_R(\mathbf{x}_R) d^2 \mathbf{x}_R, \quad (3)$$

where \mathbf{x}_B and \mathbf{x}_R must be integrated over the same area. With suitable adjustment of the beamsplitter ratios, R equals the total light intensity impinging on the object. The total instantaneous transmission function of the object can be measured as $T^{(m)} = S^{(m)}/R^{(m)}$, where m denotes the m -th measurement. Then we obtain the normalized

ghost image to be

$$\begin{aligned}
 NGI &= \left\langle \frac{SI_R(\mathbf{x}_R)}{R} \right\rangle - \left\langle \frac{S}{R} \right\rangle \langle I_R(\mathbf{x}_R) \rangle \\
 &= \langle SI'_R(\mathbf{x}_R) \rangle - \frac{\langle S \rangle}{\langle R \rangle} \langle RI'_R(\mathbf{x}_R) \rangle \\
 &\simeq C'_0 \Delta T(\mathbf{x}_R),
 \end{aligned} \tag{4}$$

where $C'_0 = A_{coh} \langle I'_R(\mathbf{x}_R) \rangle \langle I_B(\mathbf{x}_B) \rangle$ is a constant, $\Delta T(\mathbf{x}) = T(\mathbf{x}) - \langle T \rangle$, and we have assumed that $\langle T \rangle = \langle S/R \rangle \simeq \langle S \rangle / \langle R \rangle$. The normalized reference detector intensity $I'_R(\mathbf{x}_R) = I_R(\mathbf{x}_R)/R$ changes as the contrast of the speckle patterns changes, though its general kurtosis does not [9]. We now tentatively preset two threshold values $\pm T_0$ according to the value of $\langle S/R \rangle$, as illustrated in Fig. 2, which is a plot of $T^{(m)}$ against m , when all the frame intensities are recorded. The two threshold values are represented by the upper (red) and lower (blue) lines. Only the values of S/R above the upper line or below the lower line are used to trigger the CCD to take an exposure which will then be saved. Here $T_0 \in [0, \max |\delta T^{(m)}|]$, where $\delta T^{(m)} = T^{(m)} - \langle T^{(m)} \rangle$. Next, according to whether $\delta T^{(m+)} > T_0$ or $\delta T^{(m-)} < -T_0$ is satisfied, the corresponding time-correlated frames of the reference detector will be stored in Register A or B, where $m+$ and $m-$ denote all the frames larger or lower than the selected upper and lower thresholds, respectively.

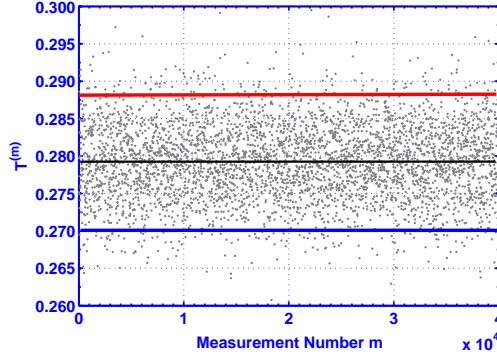


FIG. 2: (Color online). $T^{(m)}$ vs. measurement number m .

Thus we obtain

$$\left\langle \frac{\delta T_0^{(m\pm)} \delta I_R(\mathbf{x})}{|\delta T_0^{(m\pm)}|} \right\rangle_k = \begin{cases} \langle \delta I_R^{(m+)}(\mathbf{x}) \rangle_k, \\ \langle \delta I_R^{(m-)}(\mathbf{x}) \rangle_k, \end{cases} \tag{5}$$

where

$$\delta T_0^{(m\pm)} = |\delta T^{(m\pm)}| - T_0, \tag{6}$$

$$\langle \delta I_R^{(m\pm)}(\mathbf{x}) \rangle_k = \langle I_R^{(m\pm)}(\mathbf{x}) \rangle_k - \langle I_R(\mathbf{x}) \rangle, \tag{7}$$

and k denotes the number of signals $T^{(m)} - \langle T^{(m)} \rangle$ larger than T_0 or smaller than $-T_0$. Suppose that

$$\left\langle \frac{\delta T_0^{(m\pm)} \delta I_R(\mathbf{x})}{|\delta T_0^{(m\pm)}|} \right\rangle_k \simeq \frac{\langle \delta I_R(\mathbf{x}) \delta T_0^{(m\pm)} \rangle_k}{\langle |\delta T_0^{(m\pm)}| \rangle_k} \propto \pm \Delta T(\mathbf{x}). \tag{8}$$

is satisfied, this requires that $|\delta T_0^{(m\pm)}| \simeq \langle |\delta T_0^{(m\pm)}| \rangle_k$ be satisfied. It so happens that this condition is indeed satisfied due to the statistical properties of thermal light. When appropriate values of T_0 are chosen, there will be a minimum value of the deviation from the mean of the intensity fluctuation $|\delta T_0^{(m\pm)}|$, so Eq. (8) is better satisfied and the corresponding T_0 provides the optimum data for retrieving the best quality image, while at the same time both positive and negative differential images can be obtained. Thus, according to Eqs. (4), (5) and (8), the DTTCI image is given by:

$$\langle I_R^{(m+)}(\mathbf{x}) \rangle_k - \langle I_R^{(m-)}(\mathbf{x}) \rangle_k = \frac{MC'_0 \Delta T(\mathbf{x})}{2k \langle |\delta T^{(m)} - T_0| \rangle}, \tag{9}$$

where M is the total number of measurements. It is important to note that the bottleneck in the speed of GI is not only in the post-processing of the images but in the acquisition of the individual frames in the reference beam. However, the main time-consuming operation in GI is the latter, as well as the processing of all the big matrices of the reference CCD frames. The CCD exposure time is about $100 \mu\text{s}$ (10 kHz) but with only about 60 frames per second sampling rate, while an ordinary photodiode used as the bucket detector would generally have a response time on the order of ns (GHz). That is why we add a fast bucket detector in the reference beam to measure the same value of R , instead of using the same CCD to sum all the pixel intensities. This improvement should be very useful in real applications.

To implement our method, the main difficulty is how to preselect two suitable intensity threshold values relative to the average of $T^{(m)}$, since $\langle T^{(m)} \rangle$ can only be determined after all the values of T have been measured and calculated. Fortunately, we can make a rough estimate of $\langle T^{(m)} \rangle$ with only a few hundred measurements, because the intensity fluctuations of S/R are relatively small and stable for a stable thermal light source. After the two intensity values $\pm T_0$ have been preselected, as illustrated in Fig. 2, the CCD camera is triggered to record only those frames corresponding to fluctuations above T_0 or below $-T_0$, which will then be stored in registers A and B, respectively. However, these two sets of data may contain a different number of frames as the value of $\langle T \rangle$ cannot be known exactly beforehand. This asymmetry or imbalance will result in poor quality of the image retrieved by using the subtraction operation in Eq. (9). To fix this, our second step is to rearrange the values of $T^{(m)}$ in the register with the greater number of frames, in ascending or descending order, then certain measurement values closest to the mean $T^{(m)}$ are deleted such that both registers contain precisely the same number of frames. The third step is to obtain the absolute difference matrix of these two sets of data.

It should be pointed out that in our method computation time is saved not just because we only use part of the matrices, but also because we only need to add the matrices directly, rather than having first to multiply all of the differential bucket intensity signals one by one with its matching CCD matrix then integrating, as in the DGI protocol.

In the experiment, a linearly polarized 632.8 nm He-Ne laser beam is projected onto a slowly rotating (0.5 rad/s) ground-glass disk to produce a pseudothermal field of randomly varying speckles. To compare the advantages of DTTCI with other schemes, we perform measurements as in a traditional DGI experiment [26], then employ post-processing algorithms. The thermal beam is divided by a 1:1 beamsplitter (in place of BS1 in Fig. 1, with BS2 removed) into the spatially correlated object and reference beams, which have intensity distributions $I_B(\mathbf{x}_B)$ and $I_R(\mathbf{x}_R)$, respectively. Both beams are collected by identical charge-coupled device (CCD) cameras of pixel size $4.65 \mu\text{m}$. The average area of the speckles at the object and reference detector planes, which are at the same distance $z_1 = z_2 = 215 \text{ mm}$ from the source. In the experiment, both cameras capture a total of 8×10^4 frames, with a synchronized exposure time of $100 \mu\text{s}$. A digital chart of size 236×208 pixels, shown in Fig. 3(a), is centered on the bucket detector array, from which the total transmitted intensity S is calculated. The other camera is used as both the bucket detector BD2 and the reference CCD of Fig. 1, by using post-processing algorithms.

Experimental results show that the difference $|\langle S/R \rangle - \langle S \rangle / \langle R \rangle| / \langle S/R \rangle < 10^{-3}$ is always satisfied, and becomes smaller and smaller as the number of measurements M increases. We also find that the average of $\langle S/R \rangle$ can be predicted with only about a hundred measurements, for example, $\langle S/R \rangle = 0.2973$ for both $M = 120$ and $M = 40000$, as its fluctuations are small for large M . The images obtained by various methods are shown in Fig. 3. Figures 3(b), 3(c) and 3(d) were retrieved from 40000 measurements with the GI, NGI and DGI algorithms, respectively.

To implement our DTTCI scheme we perform a proof-of-principle simulation experiment. we designed the specific double threshold values in order to satisfy the very condition through a trial-and-error process. We take $\langle S/R \rangle = 0.2973$ as the average value, and set thresholds $T_{01} = 34401 \times 10^{-7}$ and $-T_{01} = -34742 \times 10^{-7}$, for a total of $20,000 \times 2$ exposures, with 20,000 frames above the positive threshold and 20,000 frames below the negative threshold. The same number but not the same 40,000 frames are used in image recovery by the other methods, for fair comparison. These 40,000 frames are sorted out from a total of 8×10^4 exposures, and the recovered ghost image is shown in Fig. 3(e), which is overall better than all the others, with especially much cleaner white parts and smoother transition in the top and bottom gray scales. The results shown in Figs. 3(f) and 3(g) are obtained by setting $T_{02} = 34300 \times 10^{-7}$, $-T_{02} = -34680 \times 10^{-7}$, and $T_{03} = 66240 \times 10^{-7}$, $-T_{03} = -65594 \times 10^{-7}$, after which 10000×2 and 4000×2 frames are chosen from a total of 4×10^4 frames, respectively. Also using 8000 frames, the image retrieved by NGI is shown in Fig. 3(h), while that retrieved by DTTCI with $\pm T_{01}$ is shown in Fig. 3(i); again we see that 3(g) and (i) are still somewhat better than (h), with clearer white parts and gray scales. Different pairs of thresholds produce different results. In our experiment the double threshold values were selected by a trial-and-error process to obtain the best images, which were derived by post-processing of the same batch of data using DGI, NGI or GI. To make sure that the numbers of frames of the reference CCD above the threshold T_0 and below $-T_0$ were the same, many threshold values were tried until exactly 20,000 frames both above and below could be obtained from the data. Actually, the choice can be done in more than one way, by arbitrary selection according to the average value of T with software, or preset from experience with hardware.

To compare the quality of images retrieved with different GI protocols, a standard normalization method has been

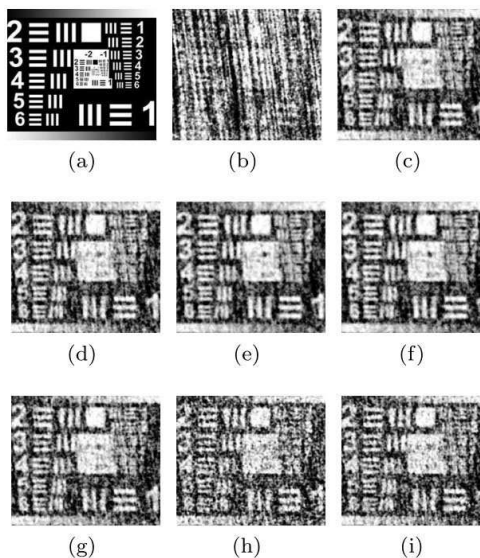


FIG. 3: (a) Digital mask Images retrieved from: (b) GI 40,000 frames, (c) NGI 40,000 frames, (d) DGI 40,000 frames, (e) DTTCI(T_{01}) 20,000 \times 2 frames, (f) DTTCI(T_{02}) 10,000 \times 2 frames, (g) DTTCI(T_{03}) 4,000 \times 2 frames, (h) NGI 8,000 frames, (i) DTTCI(T_{01}) 4,000 \times 2 frames.

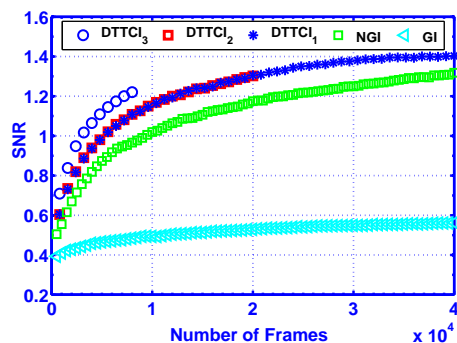


FIG. 4: (Color online). SNR vs. number of reference frames.

used, i.e., the minimum pixel value is subtracted from each matrix element of the image, then the new matrix is divided by the maximum pixel value, and the image is normalized to $[0,1]$. This is the relative intensity transmission function $t(\mathbf{x})$ of the object which we wish to retrieve and which is theoretically equal to the normalized transmission function. In addition, the Matlab image processing command [33] “*histeq*()” is used to ensure a fair and credible evaluation of the SNR of all the retrieved images.

For a quantitative comparison of the image quality, we define the SNR as [31]:

$$\text{SNR} = \frac{\text{Signal}}{\text{Noise}} = \frac{\sum_{i,j=1}^{M,N} [T_0(i,j) - \bar{T}_0]^2}{\sum_{i,j=1}^{M,N} [T(i,j) - T_0(i,j)]^2}, \quad (10)$$

where $T_0(i,j)$ and $T(i,j)$ are the transmission matrices of the object mask of size $M \times N$ and the retrieved image, respectively, and $\bar{T}_0 = (MN)^{-1} \sum_{i,j=1}^{M,N} T_0(i,j)$. The SNR values for different reconstruction methods vs. the total number of measurements, as shown in Fig. 4. The SNRs of DGI and NGI are always better than GI, which agrees with the results of Ref. 27. In all the DTTCI experiments of Fig. 3, the SNR values are larger and increase even faster than for NGI. Thus we can say that our method is better than both DGI and NGI protocols, while the image quality will increase with increase of the threshold values, and with increase of the number of measurements under the same threshold conditions.

In conclusion, we have demonstrated both theoretically and experimentally a double-threshold triggered time-correspondence imaging scheme which is insensitive to surrounding noise and has a higher SNR than that of previous

GI techniques. The technique is simple and the number of reference frames required to retrieve an image is greatly reduced, so data acquisition time is shortened. Moreover, the data processing algorithms are simpler than for DGI or NGI, consume less computing time, and require less memory storage capacity, without sacrificing image quality. With hardware implemented for triggering the reference detector at the thresholds, the total exposure and processing time could be even shorter. This new protocol offers a general approach applicable to all GI techniques, and represents a step forward towards real-time application of correlation imaging.

This work was supported by the National Basic Research Program of China (Grant No.2010CB922904), the National Natural Science Foundation of China (Grant No.60978002), and the Hi-Tech Research and Development Program of China (Grant No.2011AA120102).

-
- [1] A. V. Belinskii and D. N. Klyshko, Zh. Eksp. Teor. Fiz. **105**, 487 (1994), [Sov. Phys. JETP **78**, 259 (1994)];
 - [2] T. Pittman, Y. H. Shih, D. Strekalov, and A. Sergienko, Phys. Rev. A **52**, R3429 (1995).
 - [3] R. S. Bennink, S. J. Bentley, and R. W. Boyd, Phys. Rev. Lett. **89**, 113601 (2002);
 - [4] A. Gatti, E. Brambilla, M. Bache, and L. A. Lugiato, Phys. Rev. Lett. **93**, 093602 (2004).
 - [5] F. Ferri, D. Magatti, A. Gatti, M. Bache, E. Brambilla, and L. A. Lugiato, Phys. Rev. Lett. **94**, 183602 (2005).
 - [6] A. Valencia, G. Scarcelli, M. D. Angelo, and Y. Shih, Phys. Rev. Lett. **94**, 063601 (2005).
 - [7] G. Brida, I. P. Degiovanni, G. A. Fornaro, M. Genovese, A. Meda; Int. Journ. Quant. Inf. **9** 341 (2011);
 - [8] F. Ferri, D. Magatti, V. G. Sala, and A. Gatti, Appl. Phys. Lett. **92**, 261109 (2008).
 - [9] P. Zerom, Z. Shi, M. N. O'Sullivan, K. W. C. Chan, M. Krogstad, J. H. Shapiro, and R. W. Boyd, Phys. Rev. A **86**, 063817 (2012).
 - [10] G. Scarcelli, V. Berardi, and Y. Shih, Phys. Rev. Lett. **96**, 063602 (2006).
 - [11] A. Gatti, M. Bondani, L. A. Lugiato, M. G. A. Paris, and C. Fabre, Phys. Rev. Lett. **98**, 039301 (2007);
 - [12] J. H. Shapiro, Phys. Rev. A **78** 061802(R) (2008);
 - [13] G. Brida, M. V. Chekhova, G. A. Fornaro, M. Genovese, E. D. Lopaeva, and I. R. Berchera, Phys. Rev. A **83**, 063807 (2011).
 - [14] Y. H. Shih, Quantum Inf Process **11**:995C1001 (2012).
 - [15] J. H. Shapiro, R. W. Boyd, Quantum Inf Process **11**:1003C1011 (2012).
 - [16] N. D. Hardy and J. H. Shapiro, Phys. Rev. A **84**, 063824 (2011);
 - [17] W. Gong and S. Han, arXiv:0911.4750v3 [quant-ph] (2009);
 - [18] X. H. Chen, Q. Liu, K. H. Luo, and L. A. Wu, Opt. Lett. **34**, 695 (2009).
 - [19] J. Cheng and S. Han, Phys. Rev. Lett. **92**, 093903 (2004).
 - [20] J. Cheng, Opt. Exp. **17**, 7916-7921 (2009).
 - [21] K. W. C. Chan, D. S. Simon, A. V. Sergienko, N. D. Hardy, J. H. Shapiro, P. B. Dixon, G. A. Howland, J. C. Howell, J. H. Eberly, M. N. O'Sullivan, B. Rodenburg, and R. W. Boyd, Phys. Rev. A **84**, 043807 (2011);
 - [22] P. B. Dixon, G. A. Howland, K. W. C. Chan, C. O'Sullivan-Hale, B. Rodenburg, N. D. Hardy, J. H. Shapiro, D. S. Simon, A. V. Sergienko, R. W. Boyd, J. C. Howell, Phys. Rev. A **83**, 051803(R) (2011);
 - [23] R. Meyers, K. Deacon, and Y. H. Shih, Appl. Phys. Lett. **98**, 111115 (2011).
 - [24] W. Gong and S. Han, Opt. Lett. **36**, 394 (2011).
 - [25] M. Bina, D. Magatti, M. Molteni, A. Gatti, L. A. Lugiato, and F. Ferri, Phys. Rev. Lett. **110**, 083901 (2013).
 - [26] F. Ferri, D. Magatti, L. A. Lugiato, and A. Gatti, Phys. Rev. Lett. **104**, 253603 (2010);
 - [27] B. Q. Sun, S. Welsh, M. Edgar, J. Shapiro, and M. Padgett, Opt. Exp. **20**, 16892 (2012).
 - [28] O. Katz, Y. Bromberg, and Y. Silberberg, Appl. Phys. Lett. **95**, 131110 (2009).
 - [29] Y. Bromberg, O. Katz, and Y. Silberberg, Phys. Rev. A **79**, 053840 (2009).
 - [30] K. H. Luo, B. Q. Huang, W. M. Zheng, and L. A. Wu, Chin. Phys. Lett. **29**, 074216 (2012).
 - [31] M. F. Li, Y. R. Zhang, K. H. Luo, L. A. Wu and H. Fan. Phys. Rev. A **87**, 033813 (2013).
 - [32] X. F. Liu, X. R. Yao, W. K. Yu, G. J. Zhai, M. F. Li and L. A. Wu, AIP Advances **3** 052121 (2013).
 - [33] R. C. Gonzalez, *Digital image processing using MATLAB*, Second Edition (Prentice Hall, Upper Saddle River, NJ, 2002).